

Latent Dynamics–Aware OOD Monitoring for Trajectory Prediction with Provable Guarantees

Tongfei Guo¹ and Lili Su¹

Abstract—In safety-critical Cyber-Physical Systems (CPS), accurate trajectory prediction serves as vital guidance for downstream planning and control. Although deep learning models provide high-fidelity forecasts in the validation dataset, their reliability degrades in out-of-distribution (OOD) scenarios arising from environmental uncertainty, or rare traffic behaviors in real-world implementation. Detecting OOD events is particularly challenging because of the evolving traffic conditions and changes in interaction patterns. At the same time, formal guarantees on detection delay and false-alarm rates are critically needed due to the safety-critical nature of autonomous driving. Following recent work [1], we reframe OOD monitoring for trajectory prediction as the quickest changepoint detection (QCD) problem, which provides a principled statistical framework with well-established theory. We observe that the real-world evolution of prediction errors on in-distribution (ID) data can be well modeled by a Hidden Markov Model (HMM). Leveraging this structure, we extend the recent cumulative Maximum Mean Discrepancy approach to our setting. The resulting method avoids requiring detailed prior knowledge of the post-change distribution while admitting provable guarantees on detection delay and false-alarm rate. We validate on three real-world driving datasets, demonstrating reductions in detection delay while remaining robust to heavy-tailed distributions and unknown post-change conditions.

I. INTRODUCTION

Autonomous systems operate through a closed perception-action loop. Trajectory prediction, serving as a bridge between perception and action planning, produces exogenous signals that are consumed by downstream controllers [2]. Degradation in prediction quality can therefore undermine operating safety mechanisms—for example, it may invalidate control barrier functions or render model predictive control (MPC) problems infeasible. Concretely, consider an autonomous vehicle (AV) navigating a snow-covered intersection—a scenario that is underrepresented or absent from its training data. Such conditions introduce a distribution shift by altering road friction, visibility, and the interaction patterns of surrounding agents. Consequently, trajectory prediction models trained under nominal conditions may experience significant degradation in accuracy.

Existing approaches assess prediction reliability through anomaly detection, which aims to identify abnormal system behavior during operation. Related lines of work include out-of-distribution (OOD) detection and uncertainty quantification (UQ), which aim to characterize when model predictions may become unreliable. OOD detection methods are effective



Fig. 1: Benchmarking trajectory prediction across real-world driving datasets. Examples from nuScenes (top), ApolloScape (middle), and NGSIM (bottom) illustrate the diversity in agent interactions and scene dynamics.

for frame-wise classification in computer vision [3], but do not transfer naturally to trajectory prediction [1]. In this setting, prediction errors at individual time frames may be small yet accumulate over time as traffic interactions evolve. Where OOD detection flags anomalies at the frame level, UQ methods instead quantify predictive confidence across the sequential forecasting horizon. However, UQ methods, including Bayesian neural networks, ensembles, and Monte Carlo dropout [4–8], provide predictive confidence estimates but incur significant latency for multi-agent, multi-step forecasting. Moreover, UQ estimates often degrade under severe distribution shifts, as their calibration implicitly assumes that the training data are representative of operational conditions. In OOD traffic scenes, UQ methods may therefore produce overly confident predictions, posing potential safety risks.

Quickest change detection (QCD) offers a natural and theory-grounded solution by explicitly modeling the temporal evolution of prediction errors. Classical methods such as CUSUM provide well-established minimax guarantees on detection delay under false-alarm constraints [9–11]. Recent work has demonstrated the effectiveness of CUSUM-based methods for autonomous driving applications [1]. Moreover, [12] indicate that prediction errors in autonomous driving are inherently *multimodal*. Intuitively, the low-error mode may correspond to structured and predictable contexts, while the high-error mode may arise from complex interactions. The switches of the error modes are latent and evolve as the driving context changes, inducing temporal dependence that cannot be captured by a unimodal distribution. Hidden Markov Models (HMMs) are a large family of error evolution dynamics with varying mode/state transition probabilities and error emission distributions. They offer a robust abstrac-

*This work was not supported by any organization

¹Department of Electrical and Computer Engineering, Northeastern University, Boston, MA, USA. {guo.t, l.su}@northeastern.edu

tion for these latent modes [13, 14], and can well explain real-world patterns across multiple datasets (as can be seen in Section IV). However, their reliance on exact model specifications of both pre- and post-change distributions often limits the practical deployment of traditional QCD methods for HMM [15].

With the observation in Section IV, we extend the recent *Data-driven Cumulative Maximum Mean Discrepancy (DC-MMD)* method, which is mostly theory-oriented, to our autonomous driving problem. Unlike the original approach, which relies on a companion change-free reference sequence, we construct the reference distribution from second-order statistics of ID data, since such a sequence is unavailable in our setting. We summarize our contributions in the following:

- **Latent-aware detection.** We cast runtime OOD monitoring as a QCD problem over an HMM-driven prediction-error process and extend DC-MMD to autonomous driving, retaining lightweight computation and an optimal tradeoff between detection delay and false alarms.
- **Robustness under Heavy-Tailed.** We evaluate detection performance across light- to heavy-tailed distributions, demonstrating stable behavior even when tail assumptions are violated.
- **Robustness to Unknown Post-Change.** We show that DC-MMD does not require prior knowledge of the post-change distribution and achieves competitive detection performance compared to methods specifically designed for such settings.
- **Real-world validation.** We evaluate on nuScenes, NGSIM, and ApolloScape, demonstrating consistent improvements over benchmark baselines (i.e. sequential and UQ-based) with real-time computational overhead.

II. RELATED WORK

A. Trajectory Prediction under Distributional Shift

Modern trajectory predictors—from graph-based models such as Social-LSTM [16], GRIP++ [17], and Trajectron++ [18] to attention-based forecasters [19]—achieve strong ID accuracy, yet remains brittle under distributional shift in traffic density, topology, and interaction patterns [20, 21]. Critically, these shifts are often *silent*: predictors produce spatially coherent but inaccurate forecasts without a commensurate rise in reported uncertainty [8]. Existing robustness strategies—Deep Ensembles [4], MC-Dropout [5], energy scores [6]—quantify uncertainty at the *single-frame* level and ignore the *sequential, non-stationary* structure of deployment-time prediction errors. We bridge this gap by modeling the sequential, non-stationary prediction-error process as an HMM and applying a data-driven MMD statistic coupled with a CUSUM decision rule to detect reliability degradation as it unfolds, rather than at isolated frames.

B. OOD Detection and Sequential Change Detection

Frame-level OOD detectors [22, 23] lack temporal evidence accumulation, while classical sequential tests such as CUSUM [10] assume stationary or parametrically known

noise—an assumption that collapses in urban driving [11]. Recent variants [24] relax selected assumptions but still require a pre-specified post-change family. [12] introduces mode-aware adaptive thresholds for dynamic prediction errors yet leaving the more realistic latent non-stationary setting unaddressed.

III. PROBLEM FORMULATION

A. Trajectory Prediction

Consider an AV operating in a dynamic traffic environment. The ego vehicle continuously encounters a sequence of traffic scenes. In real-world practice, time is slotted into steps (depending on the sampling frequency). Let S^t denote the traffic scene encountered by the ego vehicle at time step $t \in \mathbb{N}$, which consists of the trajectories of neighboring vehicles and the map information in the most recent H time steps, i.e.,

$$S_t = \left\{ \{p_{t-H+1,i}, \dots, p_{t,i}\}_{i=1}^{n_t}, \mathcal{M}_{t-H+1}, \dots, \mathcal{M}_t \right\},$$

where n_t is the number of neighboring vehicles at time step t , H is the observation window length, $p_{r,i}$ is the trajectory position of vehicle i at time step r , and \mathcal{M}_r is the map for $r = t - H + 1, \dots, t$.

Let f^θ be a given trajectory predictor, and \mathcal{D} the corresponding training dataset, which is a collection of traffic scenes. The trajectory predictor maps an encountered traffic scene into predicted trajectories of neighboring vehicles, i.e.,

$$f^\theta(S_t) = \{\hat{p}_{t+1,i}, \dots, \hat{p}_{t+L,i}\}_{i=1}^{n_t},$$

where $L \in \mathbb{N}$ is the prediction window.

Prediction Error. We measure the performance of the given trajectory prediction f^θ through widely adopted metrics such as Average Displacement Error (ADE), Final Displacement Error (FDE), and Root Mean Squared Error (RMSE) [1].

Let v_t denote a target vehicle, which can be arbitrarily chosen from the neighboring vehicles. The ADE averages pointwise ℓ_2 prediction errors: $\text{ADE}_t = \frac{1}{L} \sum_{\ell=1}^L \|\hat{p}_{t+\ell,v_t} - p_{t+\ell,v_t}\|_2$. Similarly, FDE measures the ℓ_2 error in the final position: $\text{FDE}_t = \|\hat{p}_{t+L,v_t} - p_{t+L,v_t}\|_2$. RMSE is the square root of the averaged squared ℓ_2 errors: $\text{RMSE}_t = \sqrt{\frac{1}{L} \sum_{\ell=1}^L \|\hat{p}_{t+\ell,v_t} - p_{t+\ell,v_t}\|_2^2}$.

B. OOD Detection as Quickest Change-Point Detection

The prediction error can be observed online as the true trajectories are revealed sequentially. Our framework monitors the error sequence of the deployed trajectory prediction f^θ rather than raw trajectories or internal model states, making it lightweight and agnostic to the specific choice of the deployed trajectory prediction model.

Let $\{e_t\}_{t \geq 1}$ denote the sequence of prediction errors produced by the deployed predictor f^θ , where e_t may be instantiated by any of the above metrics (ADE, FDE, or RMSE). An OOD event may begin to emerge at an unknown

time step $\tau^* \in \mathbb{N} \cup \{\infty\}$; when $\tau^* = \infty$, no OOD event ever occurs. We refer to τ^* as the changepoint. Formally,

$$e_t \sim \begin{cases} f_t(\cdot), & t < \tau^*, \\ g_t(\cdot), & t \geq \tau^*, \end{cases}$$

where f_t denotes the ID error density, and g_t denotes the OOD error density. The non-stationarity of f_t and g_t arises from the inherent motion dynamics and environmental evolution that are unique to AVs (see Section IV).

Evaluation. We adopt the minimax framework for QCD [25] and evaluate detection performance through two competing objectives: detection delay and false alarm control.

We quantify detection delay via a form of *worst-case average detection delay* (WADD) [26]:

$$\text{WADD}(\tau) := \sup_{\tau^* \geq 1} \mathbb{E}_{\tau^*} [(\tau - \tau^*)^+ | \mathcal{F}_{\tau^*-1}], \quad (1)$$

where \mathcal{F}_{τ^*-1} is the natural filtration that incorporates all randomness up to the end of time step $\tau^* - 1$, $\mathbb{E}_{\tau^*}[\cdot]$ denotes expectation under the measure \mathbb{P}_{τ^*} , and the supremum ranges over all possible realizations of the changepoint. This metric helps us guard against the adversarial choice of the changepoint, which is essential for safety-critical applications.

To characterize detector stability under nominal conditions, we use the *mean time to false alarm* (MTFA):

$$\text{MTFA}(\tau) := \mathbb{E}_{\infty}[\tau], \quad (2)$$

where $\mathbb{E}_{\infty}[\cdot]$ denotes expectation when no OOD event ever occurs. Following Lorden’s optimality [25], we seek a detection method that achieves short delay subject to a prescribed false alarm constraint:

$$\tau^* \in \underset{\tau}{\text{arg min}} \text{WADD}(\tau) \quad \text{subject to} \quad \text{MTFA}(\tau) \geq \gamma, \quad (3)$$

where $\gamma > 0$ is the user-specified tolerable false alarm rate. Setting a larger γ often enforces stricter false alarm control at the cost of increased detection delay, whereas choosing a smaller γ prioritizes rapid detection.

IV. MODELING THE NON-STATIONARITY OF PREDICTION ERRORS

Prediction errors are inherently non-stationary even in the absence of OOD events. As observed in [12], the error process alternates between two latent modes: a *low-risk mode*, where predictions remain stable under routine traffic flow, and a *high-risk mode*, which emerges during complex interactions such as dense traffic, occlusions, or abrupt maneuvers. Rather than isolated spikes, the high-risk mode typically persists over several time steps as the scene evolves, reflecting the underlying traffic difficulty. HMMs provide a natural family for capturing such dynamics, where mode transition probabilities govern the temporal persistence of each regime and emission distributions characterize the error magnitude within each mode. Empirically, we observe that transitions between these modes exhibit clear Markovian structure and can be well captured by fitting HMMs to the prediction error sequences (Section IV-A).

TABLE I: Latent error dynamics across driving datasets, modeled as HMMs with emission parameters and transition probability. Emission parameters: $\Delta\mu$ (mean gap between modes) and $\bar{\sigma}^2$ (within-mode variance) characterize detection difficulty as Easy (large $\Delta\mu$, small $\bar{\sigma}^2$), Moderate (Mo, or Hard (small $\Delta\mu$, large $\bar{\sigma}^2$). Transition parameter: p (self-transition probability) reflects mode persistence. Each marker denotes the dataset source: \bullet =NGSIM, \blacktriangle =nuScenes, \star =ApolloScape.

Scene	Src	Emission		Transition
		$\Delta\mu$	$\bar{\sigma}^2$	p
<i>Highway — structured, low-density</i>				
Car-following (platoon)	\bullet	Mod.	Easy	0.15
Congested stop-and-go	\bullet	Mod.	Mod.	0.32
<i>Mixed Urban — transitional, Mod. complexity</i>				
On-ramp merge	$\blacktriangle \star$	Mod.	Mod.	0.55
Signalised intersection	$\blacktriangle \star$	Mod.	Mod.	0.50
<i>Unstructured Urban — unstructured, high-density</i>				
Unsignalised roundabout	$\blacktriangle \star$	Hard	Mod.	0.87
Unsignalised intersection	\star	Hard	Hard	0.88
Pedestrian-heavy zone	\star	Hard	Hard	0.91

A. Empirical Evidence for Dynamic-Switching Errors

We analyze error dynamics on diverse real-world datasets: NGSIM [27] (highway), nuScenes [28] (mixed urban), and ApolloScape [29] (unstructured urban). We fit Gaussian-emission HMMs with different numbers of latent states. A two-state Gaussian-emission HMM consistently provides the best empirical fit, reconfirming the two-mode observations in [12]. Table I summarizes the fitted parameters in terms of emission parameters ($\Delta\mu$, $\bar{\sigma}^2$) and transition probability (p). Our key findings are as follows:

Highway scenes (NGSIM) exhibit clearly separated low- and high-risk modes with stable dynamics and rare switching ($p \approx 0.05$). Most time steps remain in the low-risk mode, while high-risk episodes are typically triggered by abrupt maneuvers such as cut-ins or braking waves.

Urban scenes (nuScenes and ApolloScape) show more frequent switching ($p = 0.5$ – 0.9), reflecting rapidly evolving agent-agent interactions and agent-lane interactions. In these environments, the non-stationary error fluctuates as traffic conditions change.

Fig. 2 also illustrates that even within the same dataset, latent dynamics vary across scenes. Despite differences in traffic environments and prediction models, all datasets consistently exhibit such non-stationary switching. Moreover, the switching behavior varies substantially across datasets and deployed models.

B. HMM Error Model

To capture temporal dependence in prediction errors in the absence of OOD events, we model the error sequence $\{e_t\}_{t \geq 1}$ using a HMM. The key idea is that prediction errors arise from multiple latent operating conditions, which evolve over time.

Let $Z_t \in \{L, H\}$ denote the latent error mode at time t , where state L corresponds to a nominal low-error mode and state H represents an elevated-error mode. We model the

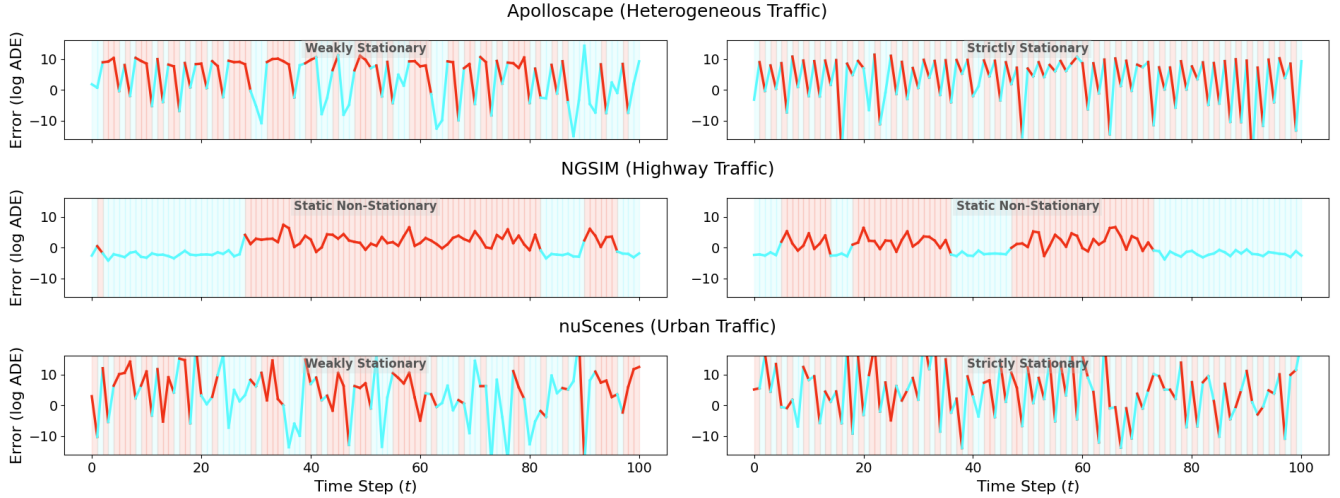


Fig. 2: Non-stationary switching behavior of prediction errors across three driving environments: NGSIM (Highway), nuScenes (Mixed Urban), and ApolloScape (Unstructured Urban). The x-axis represents the time step (t) and the y-axis denotes the error (log ADE). Preliminary results on other metrics (i.e., FDE and RMSE) show similar behaviors. Background shading indicates the inferred latent error mode: Low-Error Mode (Blue) and High-Error Mode (Red). The two modes are separated via MAP estimation under a Gaussian mixture model posterior, which assigns each observation to the component with the highest posterior responsibility.

random evolution $\{Z_t : t = 1, \dots\}$ as a Markov chain with

$$P_{ij} = \Pr(Z_{t+1} = j | Z_t = i), \quad \forall i, j \in \{L, H\}.$$

We assume $P_{ij} > 0$ for $i, j \in \{L, H\}$. Conditioned on the latent state, the observed error at each time step is drawn independently from a state-specific emission distribution:

$$e_t | Z_t = k \sim h_k, \quad k \in \{L, H\},$$

where h_L and h_H denote the low-error and high-error emission densities, respectively.

C. Pre- and Post-Change Error Models

For generality, we allow the post-change distribution g_t to follow HMM as well. Let $\Theta^{(0)} = (P^{(0)}, h_L^{(0)}, h_H^{(0)})$ and $\Theta^{(1)} = (P^{(1)}, h_L^{(1)}, h_H^{(1)})$ denote the pre- and post-change HMM parameters, respectively. This formulation captures two types of distribution shifts:

Emission shift: $h_k^{(0)} \neq h_k^{(1)}$ for some $k \in \{L, H\}$.

Transition shift: $P^{(0)} \neq P^{(1)}$, reflecting altered switching behavior between error modes.

In our experiments in Sections VI and VII, the parameters of the pre-change distribution $\Theta^{(0)}$ are learned from the training data of the deployed trajectory predictor f^θ . In particular, $P_{ij}^{(0)} > 0$ for each entry of $P^{(0)}$. We do not assume any prior knowledge of $\Theta^{(1)}$ but require that $P_{ij}^{(1)} > 0$ for $i, j \in \{L, H\}$. Instead of imposing assumptions on emission and transition shifts individually, we require that the joint distribution of $\{f_t : t = 1, \dots\}$ and the joint distribution of $\{g_t : t = 1, \dots\}$ be distinguishable, i.e.,

$$D_{KL}(f_1, f_2, \dots || g_1, g_2, \dots) > 0, \quad D_{KL}(g_1, g_2, \dots || f_1, f_2, \dots) > 0,$$

where $D_{KL}(\cdot || \cdot)$ is the Kullback–Leibler (KL) divergence.

V. METHOD: KERNEL-BASED DETECTION

To capture the information in the mode dynamics across time steps, following [26], we monitor second-order prediction errors $x_t := (e_{t-1}, e_t) \in \mathbb{R}^2$. Since each entry of $P^{(0)}$ is positive, the limiting distribution of x_t under $\Theta^{(0)}$ exists and is unique. We denote the distribution as $\lambda^{(0)}$, estimated from training data. Similarly, the limiting distribution of x_t under $\Theta^{(1)}$, denoted by $\lambda^{(1)}$, exists and is unique.

In real-world autonomous driving systems, significant uncertainty limits prior knowledge of post-change distributions. At the same time, formal performance guarantees on detection delay and false-alarm rates are often required. To address this challenge, we adapt [26] to our setting; formally described in Algorithm 1. Unlike the original approach, which relies on a companion change-free reference sequence, we construct the reference distribution from second-order statistics of ID data, since such a sequence is unavailable in our setting.

The high-level idea of DC-MMD is as follows. The error observation sequence is first partitioned into non-overlapping blocks of length m , where m is a tuning parameter. The ego vehicle then continuously evaluates the deviation between the empirical second-order error distribution and the second-order reference distribution, which is denoted by $\lambda^{(0)}$. An OOD event is declared once the cumulative deviation exceeds a pre-specified threshold b . The offset ζ is introduced to control the sensitivity to inherent observation noise.

Formally, let $\mathcal{B}_t = \{e_{(t-1)m+1}, \dots, e_{tm}\}$ denote the t -th block of the partitioned errors, which gives $m-1$ consecutive second-order samples, i.e., x_t^1, \dots, x_t^{m-1} . Let $\hat{\mu}_t$ denote the empirical second-order distribution over the t -th block.

To compare $\hat{\mu}_t$ and $\lambda^{(0)}$, we use MMD in a Reproducing Kernel Hilbert Space (RKHS). Let $k(\cdot, \cdot)$ be a bounded kernel with associated RKHS \mathcal{H} . The MMD between $\hat{\mu}_t$ and $\lambda^{(0)}$,

Algorithm 1 Data-driven Cumulative Maximum Mean Discrepancy (DC-MMD)

- 1: **Input:** second-order error distribution of ID data $\lambda^{(0)}$, block length m , offset ζ , threshold b
 - 2: **Initialize:** $W_0 \leftarrow 0$, $\mathcal{B}_0 \leftarrow \mathcal{O}$
 - 3: **for** $t = 1, \dots$ **do**
 - 4: observe a prediction error e_t
 - 5: construct the second-order sample $x_t = (e_{t-1}, e_t)$
 - 6: $\mathcal{B}_t \leftarrow \mathcal{B}_{t-1} \cup \{x_t\}$
 - 7: **if** $|\mathcal{B}_t| \bmod m = 0$ **then**
 - 8: construct the empirical distribution $\hat{\mu}_{\lfloor t/m \rfloor}$
 - 9: compute $D(\hat{\mu}_{\lfloor t/m \rfloor}, \lambda^{(0)})$
 - 10: $W_{\lfloor t/m \rfloor} \leftarrow \max\{0, W_{\lfloor t/m \rfloor - 1} + D(\hat{\mu}_{\lfloor t/m \rfloor}, \lambda^{(0)}) - \zeta\}$
 - 11: **if** $W_{\lfloor t/m \rfloor} > b$ **then**
 - 12: declare an OOD event and **break**
 - 13: **end if**
 - 14: $\mathcal{B}_t \leftarrow \mathcal{O}$
 - 15: **end if**
 - 16: **end for**
-

denoted by $D(\hat{\mu}_t, \lambda^{(0)})$, can be computed as

$$D^2(\hat{\mu}_t, \lambda^{(0)}) = \mathbb{E}_{X, \bar{X} \sim \hat{\mu}_t} [k(X, \bar{X})] + \mathbb{E}_{Y, \bar{Y} \sim \lambda^{(0)}} [k(Y, \bar{Y})] - 2\mathbb{E}_{X \sim \hat{\mu}_t, Y \sim \lambda^{(0)}} [k(X, Y)],$$

where X, \bar{X} are independent copies that follow $\hat{\mu}_t$, and Y, \bar{Y} are independent copies that follow $\lambda^{(0)}$.

An occurrence of an OOD event is declared when

$$\tau(b) = \inf \left\{ mt : \max_{1 \leq i \leq t} \sum_{j=i}^t (D(\hat{\mu}_j, \lambda^{(0)}) - \zeta) > b \right\}, \quad (4)$$

where $0 < \zeta < D(\lambda^{(1)}, \lambda^{(0)})$, and $W^t := \max_{1 \leq i \leq t} \sum_{j=i}^t (D(\hat{\mu}_j, \lambda^{(0)}) - \zeta)$ can be computed in an iterative fashion:

$$W^t = \max\{0, W^{t-1} + (D(\hat{\mu}_t, \lambda^{(0)}) - \zeta)\}.$$

Using MMD in an RKHS ensures the boundedness of the associated random quantities, which in turn enables the application of tools from random process theory (such as Doob's martingale inequality) to derive concentration results.

Remark 1 (Optional Variance-Normalization): The finite-sample variance of $D(\hat{\mu}_t, \lambda^{(0)})$ may vary substantially across datasets and across different on-board trajectory predictors. For practical implementation and easier selection of the detection threshold b , one may optionally normalize the block increment as $\frac{D(\hat{\mu}_t, \lambda^{(0)}) - \zeta}{\sqrt{\hat{\sigma}_t + \varepsilon}}$, where $\hat{\sigma}_t$ is estimated from a rolling window of recent blocks, and $\varepsilon > 0$ is a small constant introduced to ensure numerical stability.

Let $\Delta^{(0)} \in [0, 1)$ denote the spectral gap of the transition matrix associated with the second-order Markov chain under $\Theta^{(0)}$, and let $R^{(0)} := \sup_x \mathbb{E}[k(x, X')^2]$, where $X' \sim \lambda^{(0)}$, be the second-moment envelope of the kernel. Both $\Delta^{(0)}$ and $R^{(0)}$ enter the concentration bound for the blockwise MMD estimator and appear in the detection-delay guarantee (Theorem 1).

Theorem 1 (Detection delay): For any given $b > 0$, $m \in \mathbb{N}$, and properly chosen ζ such that $\zeta < D(\lambda^{(1)}, \lambda^{(0)})$, the WADD of Algorithm 1 satisfies

$$\text{WADD}(\tau(b)) \leq \frac{mb}{(\sqrt{d} - \sqrt{a})^2} + \frac{m\sqrt{d}}{\sqrt{d} - \sqrt{a}},$$

where $a = \sqrt{\frac{2-2\Delta^{(0)}+4R^{(0)}}{(m-1)(1-\Delta^{(0)})}}$, and $d = D(\lambda^{(1)}, \lambda^{(0)}) - \zeta$.

Proof: Theorem 1 follows directly from the analysis of [26, Theorem 1] by setting a_P , as defined therein, to zero.

It is worth noting that if, instead of allowing b to be an arbitrary positive number, we restrict b to a collection of values (possibly of infinite cardinality) such that a certain intermediate quantity in the analysis of [26, Theorem 1] becomes an integer, then the upper bound in Theorem 1 can be further simplified to $\text{WADD}(\tau(b)) \leq \frac{mb}{(\sqrt{d} - \sqrt{a})^2}$. ■

Theorem 2 (False alarm): [26] For any given b, m , and properly chosen ζ such that $\zeta < D(\lambda^{(1)}, \lambda^{(0)})$, the MTFA of Algorithm 1 grows exponentially in c , formally

$$\text{MTFA}(\tau(b)) \geq m \exp(qb),$$

where $q > 0$ is a constant that depends on a and ζ but is independent of b .

Remark 2 (Order-optimality): As noted in [26], exponential growth of $\text{WADD}(\tau(b))$ is desirable. This is because, to satisfy a given false-alarm constraint $\text{WADD}(\tau(b)) \geq \gamma$ for some $\gamma > 0$, one may choose $b = \frac{\log \gamma - \log m}{q}$, assuming that γ is a constant that does not depend on other problem parameters. By Theorem 1, we know that Algorithm 1 achieves a detection delay of $O(\frac{\log \gamma - \log m}{q})$, which matches the order-wise lower bound $O(\log \gamma)$ for a broad region of γ . Hence, Algorithm 1 achieves order optimality.

VI. EXPERIMENTAL SETUP

Datasets. We evaluate DC-MMD across three complementary real-world driving domains: NGSIM [27] (structured highway, US-101 and I-80), nuScenes [28] (mixed urban traffic, Boston and Singapore), and ApolloScape [29] (unstructured dense urban, Beijing).

Trajectory prediction models. We evaluate two representative trajectory predictors: GRIP++ [17] (graph-based relational modeling) and FQA [19] (attention-based spectral modeling). The two architectures belong to distinct paradigm families. Consistent DC-MMD performance across both architecturally distinct paradigms confirms model-agnostic runtime monitoring.

Baselines. All methods operate on the identical scalar prediction error sequence $\{e_t\}$ without model introspection or repeated forward passes. We compare against classic UQ-based detection (NLL [22], IGMM [23]), and sequential change detectors: Classical G-CUSUM [10], GMM-CUSUM [1], and Mode-Aware CUSUM [12].

Evaluation Metrics. Following the Lorden minimax formulation (Sec. III), we report WADD (Eq. (1)) and MTFA (Eq. (2)) as primary metrics, with AUROC and FPR@95 included for threshold-free comparison.

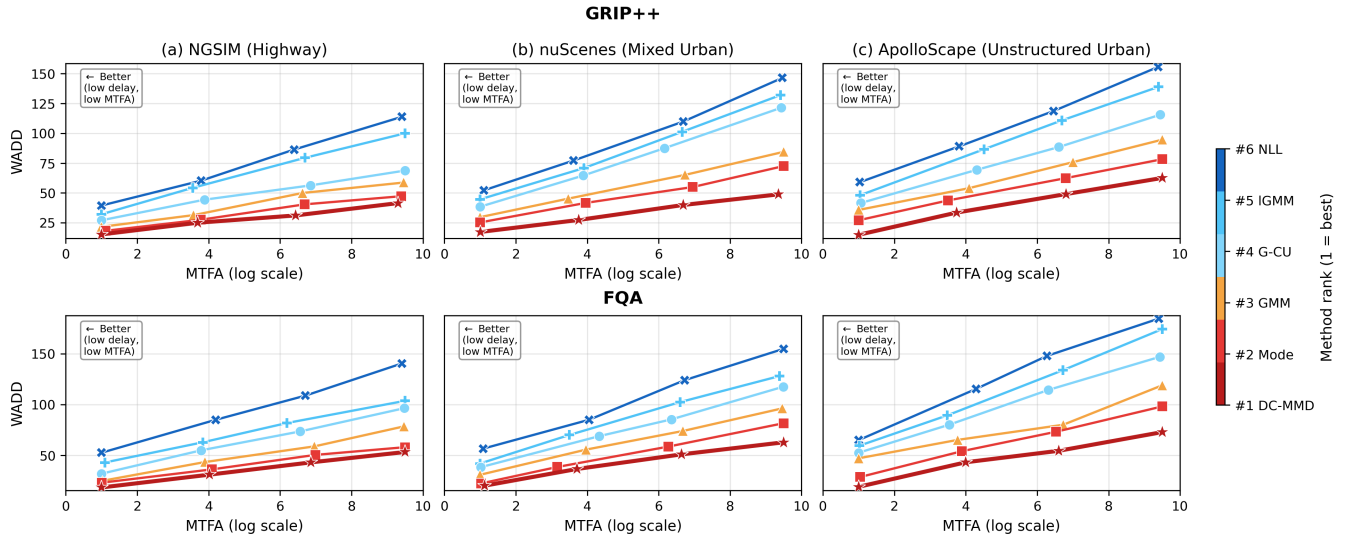


Fig. 3: WADD–MTFA trade-off curves across driving domains. Each curve traces one detection method under two models: GRIP++ (top) and FQA (bottom) prediction. WADD ↓ = faster detection; MTFA ↑ = fewer false alarms.

TABLE II: OOD detection performance across datasets. Higher AUROC (↑) and lower FPR@95 (↓) indicate better performance.

Category	Method	AUROC ↑			FPR@95 ↓		
		NGSIM (Highway)	nuScenes (Mixed urban)	ApolloScope (Unstructured Urban)	NGSIM (Highway)	nuScenes (Mixed urban)	ApolloScope (Unstructured Urban)
Point-wise (UQ-based)	NLL [30]	0.71	0.64	0.58	0.62	0.71	0.78
	IGMM [23]	0.74	0.69	0.62	0.57	0.65	0.73
Sequential	G-CUSUM [10]	0.82	0.76	0.69	0.44	0.52	0.61
	GMM-CUSUM [1]	0.85	0.79	0.73	0.41	0.48	0.56
	Mode-CUSUM [12]	0.88	0.82	0.77	0.36	0.43	0.51
	DC-MMD (ours)	0.93	0.89	0.84	0.24	0.31	0.39

OOD Scene Generation. Following controlled-shift methodologies in [31], we construct *subtle OOD* scenes by applying bounded perturbations to observed trajectories. Velocity, acceleration, and jerk are constrained within $\mu \pm 3\sigma$ of the training distribution, while spatial deviation at each trajectory point is limited to 1 m to preserve lane consistency and interaction realism. These constraints ensure the resulting scenes remain dynamically feasible while exhibiting distributional characteristics different from the ID setting, mimicking subtle shifts in driving conditions that can degrade trajectory prediction accuracy. As shown in Table III, small trajectory perturbations (avg. ≈ 0.5 m) already produce substantial degradation in prediction accuracy across datasets and models, reflecting real-world situations where underrepresented or unexpected environmental factors subtly alter vehicle dynamics and interaction patterns.

Implementation Details. All methods operate on the same scalar error sequence to ensure fair comparison. The hyperparameters of DC-MMD (Algorithm 1) are set as follows. The block length is set to $m=50$ (≈ 5 s at 10 Hz), selected from $\{25, 50, 75, 100\}$ as the best-performing value in our experiments. The kernel k is a Gaussian RBF with bandwidth $\sigma=0.8$ chosen by [32]. The offset $\zeta=0.05$, corresponding to the sample mean of MMD values on ID blocks, so that the CUSUM statistic W_t has a negative drift under nominal

TABLE III: Impact of subtle OOD generation on prediction accuracy. Dev. denotes the average spatial shifts (≤ 1 m). Δ (%) denotes the error (ADE) increase from ID to OOD setting.

Dataset	Model	Dev. (m)	ADE (ID/OOD)	Δ (%)
NGSIM	GRIP++	0.46	0.73/1.82	+149
	FQA	0.44	0.81/2.05	+153
nuScenes	GRIP++	0.52	1.12/2.71	+142
	FQA	0.49	1.24/3.01	+143
ApolloScope	GRIP++	0.55	1.48/3.74	+153
	FQA	0.53	1.61/4.02	+150
Average		0.50	1.17/2.89	+148

* Similar trends are observed for FDE and RMSE.

operation. For the detection delay versus false alarm trade-off curves, the threshold b is swept over a range so that all methods are compared at matched MTFA.

VII. RESULTS

For conciseness, results are reported using GRIP++ with ADE as the representative predictor–metric pair. Similar trends hold across other configurations.

A. How does DC-MMD compare with baselines across predictors and driving domains?

We evaluate this question using detection accuracy (Table II), delay–false-alarm trade-offs (Fig. 3), and robustness

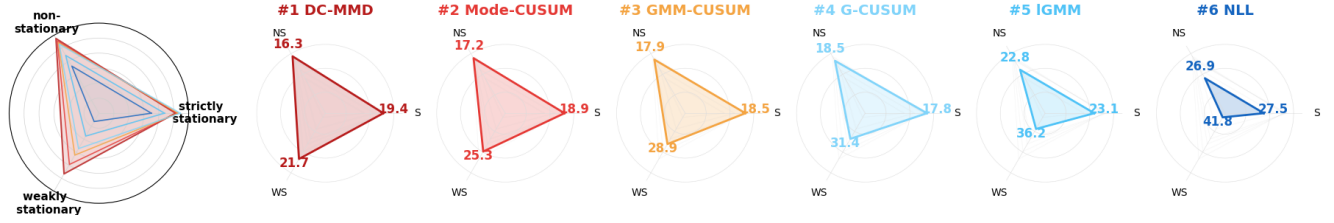


Fig. 4: Latent-dynamic performance across benchmarks. Each radar axis represents a progressively weaker stationarity assumption, arranged clockwise: **S** (strictly stationary) \rightarrow **WS** (weakly stationary) \rightarrow **NS** (non-stationary). The Global Profile (left) overlays all six methods; individual panels isolate each method’s footprint with per-axis average WADD annotated (at MTFA \approx 2 ; 500 runs). Larger area \Leftrightarrow WADD \downarrow (faster change-point response).

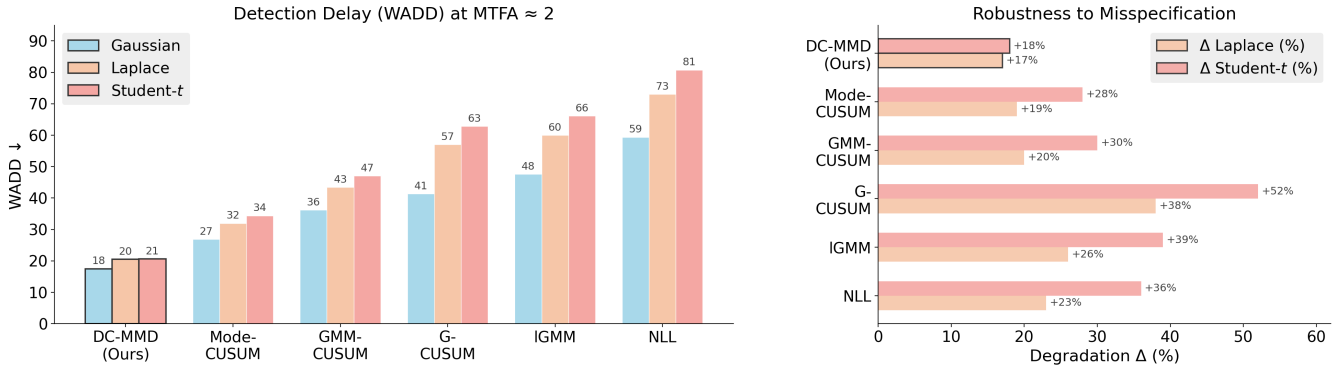


Fig. 5: Robustness to heavy-tailed distribution. *Left*: Detection delay (WADD) at MTFA \approx 2. DC-MMD (Ours) maintains the lowest delay across all distributions: Gaussian (light-tailed, blue), Laplace (moderate-tailed, tan), and Student- t (heavy-tailed, red).

TABLE IV: Detection delay (WADD) at MTFA \approx 2 under heavy-tailed emission misspecification. Δ (%) denotes degradation relative to the Gaussian baseline.

Method	WADD \downarrow			Δ (%)	
	Gaussian	Laplace	Student- t	LP	ST
DC-MMD (Ours)	17.52	20.50	20.67	+17	+18
Mode-CUSUM	26.87	31.97	34.39	+19	+28
GMM-CUSUM	36.18	43.42	47.03	+20	+30
G-CUSUM	41.35	57.06	62.85	+38	+52
IGMM	47.58	59.95	66.14	+26	+39
NLL	59.39	73.05	80.77	+23	+36

* LP = Laplace, ST = Student- t .

under different latent dynamics (Fig. 4). DC-MMD consistently achieves the strongest detection accuracy across all domains, reaching AUROC 0.84 on the Unstructured Urban ApolloScape dataset while reducing FPR@95 relative to sequential baselines such as Mode-CUSUM; in contrast, point-wise methods (NLL, IGMM) remain near 0.6 AUROC, indicating limited capability under high-entropy scenes. The delay–false-alarm frontier in Fig. 3 shows that DC-MMD reduces WADD by roughly 15–35% across NGSIM, nuScenes, and ApolloScape while maintaining comparable MTFA. Finally, Fig. 4 demonstrates that DC-MMD sustains the lowest detection delay across i.i.d., static multi-modal, and Markov-switching regimes, whereas classical detectors degrade substantially under switching dynamics.

B. How robust is DC-MMD under heavy-tailed distribution?

Table IV evaluates robustness to heavy-tailed emission misspecification at a fixed operating point (MTFA \approx 2). DC-

TABLE V: Detection delay when the post-change distribution is unknown. All methods operate at MTFA \approx 1. Results are averaged over 500 independent runs. Robust CUSUM uses a shift-based surrogate with $\kappa=2$ selected following [1].

Method	Robust	Delay
DC-MMD (Ours)	✓	16.7
Robust CUSUM (κ -shift)	✓	16.4
G-CUSUM (misspecified)		25.8
NLL		32.6

TABLE VI: Computational Complexity and Real-Time Suitability.

Method	Complexity (Per Step)	Parameters	Real-Time
NLL [22]	$O(1)$	0	***
G-CUSUM [10]	$O(1)$	0	***
IGMM [23]	$O(1)$	Low	***
Deep Ensembles [4]	$O(N)$	$N \times$ Model	*
DC-MMD (Ours)	$O(1)^\ddagger$	Minimal	***

*** Excellent (< 0.01 ms), * Low (> 10 ms).

\ddagger Achieved via recursive sliding-window MMD updates.

MMD already achieves the lowest detection delay. Under Laplace and Student- t emissions, performance degradation becomes more pronounced for likelihood-based detectors. For example, G-CUSUM increases delay by 38% and 52%, indicating strong sensitivity to heavy-tailed errors. Mode-CUSUM and GMM-CUSUM provide partial robustness but still degrade by 19–30%. In contrast, DC-MMD maintains stable performance, with delay increases limited to only 6% and 9% (Fig. 5).

C. How robust is DC-MMD to unknown post-change distributions?

We further investigate robustness when the post-change distribution is unknown. Unlike methods that rely on parametric assumptions about the post-change regime, DC-MMD operates without requiring any such prior knowledge. To compare against baselines designed for this setting, we include Robust CUSUM, which assumes a minimal location shift $\kappa=2$ following [1], as a robust baseline, alongside G-CUSUM and NLL, which lack a robust design. As shown in Table V, DC-MMD and Robust CUSUM achieve comparable delays (16.7 and 16.4), both effectively handling distributional uncertainty. G-CUSUM incurs a higher delay (25.8) because its likelihood ratio becomes misspecified when the post-change distribution deviates from the assumed model. NLL exhibits the largest delay (32.6) as it lacks the optimal stopping structure of CUSUM-type methods. These results highlight the practical advantage of DC-MMD in scenarios where post-change characteristics are rarely known in advance.

D. Is DC-MMD deployable under real-time constraints?

To evaluate the feasibility of DC-MMD for high-frequency robotics, we compare its per-step computational overhead against baselines in Table VI. Our design is decoupled from the primary model's parameter space, ensuring constant-time inference regardless of the predictor's depth.

VIII. CONCLUSION AND DISCUSSION

We presented DC-MMD, a latent-aware sequential change detection framework for runtime monitoring of trajectory prediction. By combining an HMM with a CUSUM stopping rule, the method captures latent error dynamics in prediction residuals. Across NGSIM, nuScenes, and ApolloScape, DC-MMD reduces detection delay by 15–35% compared with the strongest sequential baseline, while maintaining stable performance under misspecification and matching robust baselines in distribution-free settings, with $O(1)$ per-step cost. Future work will extend the framework to incorporate perception-level signals and to connect detection with planner-level fallback strategies for end-to-end runtime assurance.

REFERENCES

- [1] T. Guo, T. Banerjee, R. Liu, and L. Su, "Building real-time awareness of out-of-distribution in trajectory prediction for autonomous vehicles," *ACM Transactions on Cyber-Physical Systems*, 2026.
- [2] H. Wei and Y. Shi, "Mpc-based motion planning and control enables smarter and safer autonomous marine vehicles: Perspectives and a tutorial survey," *IEEE/CAA Journal of Automatica Sinica*, vol. 10, no. 1, pp. 8–24, 2022.
- [3] Y. Feng, D. J. X. Ng, and A. Easwaran, "Improving variational autoencoder based out-of-distribution detection for embedded real-time applications," *ACM Transactions on Embedded Computing Systems (TECS)*, vol. 20, no. 5s, pp. 1–26, 2021.
- [4] B. Lakshminarayanan, A. Pritzel, and C. Blundell, "Simple and scalable predictive uncertainty estimation using deep ensembles," *Advances in neural information processing systems*, vol. 30, 2017.
- [5] Y. Gal and Z. Ghahramani, "Dropout as a bayesian approximation: Representing model uncertainty in deep learning," in *international conference on machine learning*. PMLR, 2016, pp. 1050–1059.
- [6] W. Liu, X. Wang, J. Owens, and Y. Li, "Energy-based out-of-distribution detection," *Advances in neural information processing systems*, vol. 33, pp. 21 464–21 475, 2020.
- [7] K. Wang, C. Shen, X. Li, and J. Lu, "Uncertainty quantification for safe and reliable autonomous vehicles: A review of methods and applications," *IEEE Transactions on Intelligent Transportation Systems*, 2025.
- [8] J. Yang, K. Zhou, Y. Li, and Z. Liu, "Generalized out-of-distribution detection: A survey," *International Journal of Computer Vision*, vol. 132, pp. 5635–5662, 2024.
- [9] A. Tartakovsky, I. Nikiforov, and M. Basseville, *Sequential analysis: Hypothesis testing and changepoint detection*. CRC press, 2014.
- [10] E. S. Page, "Continuous inspection schemes," *Biometrika*, vol. 41, no. 1/2, pp. 100–115, 1954.
- [11] M. Basseville, I. V. Nikiforov *et al.*, *Detection of abrupt changes: theory and application*. prentice Hall Englewood Cliffs, 1993, vol. 104.
- [12] T. Guo and L. Su, "Dynamic aware: Adaptive multi-mode out-of-distribution detection for trajectory prediction in autonomous vehicles," *arXiv preprint arXiv:2509.13577*, 2025.
- [13] B. Mor, S. Garhwal, and A. Kumar, "A systematic review of hidden markov models and their applications: B. mor *et al.*" *Archives of computational methods in engineering*, vol. 28, no. 3, pp. 1429–1448, 2021.
- [14] C.-D. Fuh and A. G. Tartakovsky, "Asymptotic bayesian theory of quickest change detection for hidden markov models," *IEEE Transactions on Information Theory*, vol. 65, no. 1, pp. 511–529, 2018.
- [15] C.-D. Fuh and Y. Mei, "Quickest change detection and kullback-leibler divergence for two-state hidden markov models," *IEEE Transactions on Signal Processing*, vol. 63, no. 18, pp. 4866–4878, 2015.
- [16] A. Alahi, K. Goel, V. Ramanathan, A. Robicquet, L. Fei-Fei, and S. Savarese, "Social lstm: Human trajectory prediction in crowded spaces," in *CVPR*, 2016.
- [17] X. Li, X. Ying, and M. C. Chuah, "GRIP++: Enhanced graph-based interaction-aware trajectory prediction for autonomous driving," *arXiv preprint arXiv:1907.07792*, 2020.
- [18] T. Salzmann, B. Ivanovic, P. Chakravarty, and M. Pavone, "Trajectron++: Dynamically-feasible trajectory forecasting with heterogeneous data," in *ECCV*, 2020.
- [19] F. Juliari, A. Seff, F. Galasso *et al.*, "Transformer networks for trajectory forecasting," in *ICRA*, 2021.
- [20] A. Filos, P. Tigkas, R. McAllister, N. Rhinehart, S. Levine, and Y. Gal, "Can autonomous vehicles identify, recover from, and adapt to distribution shifts?" in *International Conference on Machine Learning*. PMLR, 2020, pp. 3145–3153.
- [21] B. Stoler, I. Navarro, M. Jana, S. Hwang, J. Francis, and J. Oh, "SafeShift: Safety-informed distribution shifts for robust trajectory prediction in autonomous driving," in *2024 IEEE Intelligent Vehicles Symposium (IV)*. IEEE, 2024, pp. 1179–1186.
- [22] D. Hendrycks and K. Gimpel, "A baseline for detecting misclassified and out-of-distribution examples in neural networks," in *Proceedings of the International Conference on Learning Representations (ICLR)*, 2017.
- [23] J. Wiederer, J. Schmidt, U. Kressel, K. Dietmayer, and V. Belagiannis, "Joint out-of-distribution detection and uncertainty estimation for trajectory prediction," in *2023 IEEE/RSJ International Conference on Intelligent Robots and Systems (IROS)*. IEEE, 2023, pp. 5487–5494.
- [24] N. Ahad, M. A. Davenport, and Y. Xie, "Data-adaptive symmetric CUSUM for sequential change detection," *Sequential Analysis*, vol. 43, no. 1, pp. 1–27, 2024.
- [25] G. Lorden, "Procedures for reacting to a change in distribution," *The annals of mathematical statistics*, pp. 1897–1908, 1971.
- [26] Q. Zhang, Z. Sun, L. C. Herrera, and S. Zou, "Data-driven quickest change detection in (hidden) markov models," *IEEE Transactions on Signal Processing*, vol. 72, pp. 5567–5580, 2024.
- [27] Federal Highway Administration. (2020) Traffic analysis tools: Next generation simulation. [Accessed: Sep. 13, 2024]. [Online]. Available: <https://ops.fhwa.dot.gov/trafficanalysis/tools/ngsim.htm>
- [28] H. Caesar, V. Bankiti, A. H. Lang, S. Vora, V. E. Liong, Q. Xu, A. Krishnan, Y. Pan, G. Baldan, and O. Beijbom, "nusenes: A multimodal dataset for autonomous driving," in *Proceedings of the IEEE/CVF conference on computer vision and pattern recognition*, 2020, pp. 11 621–11 631.
- [29] X. Huang, X. Cheng, Q. Geng, B. Cao, D. Zhou, P. Wang, Y. Lin, and R. Yang, "The apolloScape dataset for autonomous driving," in *Proceedings of the IEEE conference on computer vision and pattern recognition workshops*, 2018, pp. 954–960.

- [30] K. Lee, K. Lee, H. Lee, and J. Shin, "A simple unified framework for detecting out-of-distribution samples and adversarial attacks," *Advances in neural information processing systems*, vol. 31, 2018.
- [31] Q. Zhang, S. Hu, J. Sun, Q. A. Chen, and Z. M. Mao, "On adversarial robustness of trajectory prediction for autonomous vehicles," in *Proceedings of the IEEE/CVF Conference on Computer Vision and Pattern Recognition*, 2022, pp. 15 159–15 168.
- [32] A. Gretton, K. M. Borgwardt, M. J. Rasch, B. Schölkopf, and A. Smola, "A kernel two-sample test," *The journal of machine learning research*, vol. 13, no. 1, pp. 723–773, 2012.